PAPER

Toward a burning plasma state using diamond ablator inertially confined fusion (ICF) implosions on the National Ignition Facility (NIF)

To cite this article: L Berzak Hopkins *et al* 2019 *Plasma Phys. Control. Fusion* **61** 014023

IOP Publishing Plasma Physics and Controlled Fusion
Plasma Phys. Control. Fusion **61** (2019) 014023 (10pp) https://doi.org/10.1088/1361-6587/aad97e

Toward a burning plasma state using diamond ablator inertially confined fusion (ICF) implosions on the National Ignition Facility (NIF)

L Berzak Hopkins[1,7], S LePape[1], L Divol[1], A Pak[1], E Dewald[1], D D Ho[1], N Meezan[1], S Bhandarkar[1], L R Benedetti[1], T Bunn[1], J Biener[1], J Crippen[2], D Casey[1], D Clark[1], D Edgell[3], D Fittinghoff[1], M Gatu-Johnson[4], C Goyon[1], S Haan[1], R Hatarik[1], M Havre[2], D Hinkel[1], H Huang[2], N Izumi[1], J Jaquez[2], O Jones[1], S Khan[1], A Kritcher[1], C Kong[2], G Kyrala[5], O Landen[1], T Ma[1], A MacPhee[1], B MacGowan[1], A J Mackinnon[1], M Marinak[1], J Milovich[1], M Millot[1], P Michel[1], A Moore[1], S R Nagel[1], A Nikroo[1], P Patel[1], J Ralph[1], H Robey[1], J S Ross[1], N G Rice[2], S Sepke[1], V A Smalyuk[1], P Sterne[1], D Strozzi[1], M Stadermann[1], P Volegov[5], C Weber[1], C Wild[6], C Yeamans[1], D Callahan[1], O Hurricane[1], R P J Town[1] and M J Edwards[1]

[1] Lawrence Livermore National Laboratory, Livermore, CA, United States of America
[2] General Atomics, San Diego, CA, United States of America
[3] Laboratory for Laser Energetics, University of Rochester, Rochester, NY, United States of America
[4] Plasma Science and Fusion Center, Mass. Institute of Technology, Cambridge, MA, United States of America
[5] Los Alamos National Laboratory, Los Alamos, NM, United States of America
[6] Diamond Materials GmbH, Freiburg, Germany

E-mail: hopkins31@llnl.gov

Received 3 July 2018, revised 2 August 2018
Accepted for publication 10 August 2018
Published 21 November 2018

Abstract

Producing a burning plasma in the laboratory has been a long-standing milestone for the plasma physics community. A burning plasma is a state where alpha particle deposition from deuterium–tritium (DT) fusion reactions is the leading source of energy input to the DT plasma. Achieving these high thermonuclear yields in an inertial confinement fusion (ICF) implosion requires an efficient transfer of energy from the driving source, e.g., lasers, to the DT fuel. In indirect-drive ICF, the fuel is loaded into a spherical capsule which is placed at the center of a cylindrical radiation enclosure, the hohlraum. Lasers enter through each end of the hohlraum, depositing their energy in the walls where it is converted to x-rays that drive the capsule implosion. Maintaining a spherically symmetric, stable, and efficient drive is a critical challenge and focus of ICF research effort. Our program at the National Ignition Facility has steadily resolved challenges that began with controlling ablative Rayleigh–Taylor instability in implosions, followed by improving hohlraum-capsule x-ray coupling using low gas-fill hohlraums, improving control of time-dependent implosion symmetry, and reducing target engineering feature-generated perturbations. As a result of this program of work, our team is now poised to enter the burning plasma regime.

Keywords: inertial confinement fusion, laser, diamond, symmetry control, hohlraum

(Some figures may appear in colour only in the online journal)

[7] Author to whom any correspondence should be addressed.

1. Introduction

The goal of inertial confinement fusion (ICF) is to compress hydrogenic species (deuterium and tritium, DT) to high pressure conditions such that the DT fuses and releases large amounts of energy. To reach fusion-relevant conditions, the DT fuel is cryogenically frozen inside a low-Z capsule; the capsule outer surface is ablated driving the remaining capsule material and fuel inwards to high densities, temperatures, and pressures. In indirect-drive ICF, the capsule is placed at the center of a radiation enclosure (hohlraum), and lasers are fired into the hohlraum, depositing their energy and forming an x-ray drive which serves to ablate and implode the fuel-filled capsule [1].

The energy released from fusing DT takes the form of a 14.1 MeV neutron and a 3.5 MeV alpha particle (^{4}He). If the implosion density and pressure are high enough, this alpha particle deposits its kinetic energy via small angle scattering, raising the temperature of the fusion plasma and leading to a feedback cycle of self-heating. On the path toward reaching such a propagating burn front and ignition, there are several distinct performance steps that must be surmounted, and key improvements in understanding have steadily led to platform design changes that allow these steps to be reached. Recent experiments have reached a new step of fusion energy output greater than the kinetic energy of the imploding shell (figure 1 pink markers) [2], nearing the burning plasma regime. We report here the detailed laser design and symmetry control techniques utilized to reach this milestone and how these are planned for future utilization to reach the next stage of implosion performance.

Burning plasmas and ignition require compression to high pressure and temperatures in short time scales to reach self-heating conditions, where heating from alpha particle deposition is the dominant source of heating (burning plasma, slightly higher than current implosions as can be seen in figure 1) and where energy output from fusion reactions is greater than the cooling from conduction and x-ray losses (ignition). The implosion nuclear yield (Y) is a function of the stagnation pressure ($P_{\rm stag}$), core temperature ($T_{\rm hotspot}$), core volume (V), and confinement time (τ) [3]:

$$Y \propto P_{\rm stag}^2 T_{\rm hs}^2 V\tau. \tag{1}$$

This equation can be recast into terms controlled by target platform design to understand the distinct contributions to performance (described in further detail in an appendix to [7])

$$P_{\rm stag} \propto p_{\rm abl}^{2/5} \frac{v_{\rm imp}^3}{\alpha^{0.9}} \epsilon, \tag{2}$$

$$T_{\rm hs} \propto v_{\rm imp}^{4/3} \tag{3}$$

such that:

$$Y \propto p_{\rm abl}^{4/5} \frac{v_{\rm imp}^{7.7}}{\alpha^{1.8}} \epsilon S^{4.4}, \tag{4}$$

where $p_{\rm abl}$ is the capsule ablation pressure generally set by the choice of ablator (capsule) material and the internal hohlraum temperature; $v_{\rm imp}$ is the implosion velocity, a direct function of the laser energy converted to x-rays available to drive the implosion and capsule mass; α is a pressure ratio encompassing the entropy contained in the DT fuel and serves to

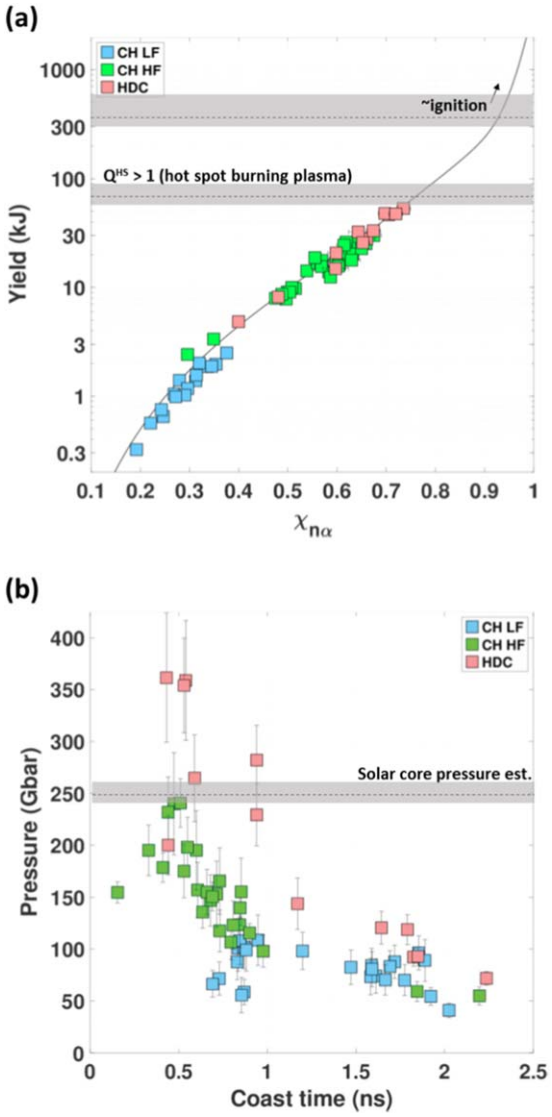

Figure 1. (a) Measured fusion yield output relative to an ignition threshold metric (which convolves implosion areal density with fusion yield and fuel mass as defined in [4]) with an estimate for burning plasma and ignition levels as described in [5]; (b) implosion pressure inferred from experimental measurements relative to the laser design metric 'coast time', the time between the end of the laser pulse and peak neutron emission compared with an estimate for the pressure at the center of the sun [6]. Blue markers denote ICF implosions on NIF from 2009–2012, which were limited in performance by ablative Rayleigh–Taylor (RT) instabilities, asymmetries, and shell perforations. Green markers denote implosions from 2013–2015, which implemented a laser design that mitigated RT instability but remained limited by implosion asymmetries and perforation of the shell by engineering features as well as laser energy. Pink markers denote recent high density carbon (HDC or 'diamond') 2016–2017 implosions with improved coupling, reduced laser-plasma interaction effects, and time-dependent symmetry control through the use of low gas-fill density in the hohlraum. The highest performing implosions, to-date, also included smaller fuel fill tubes, reducing the impact of that particular target engineering feature.

quantify the compressibility of the implosion [8]; ϵ is an effective efficiency term which takes into account implosion energy loss mechanisms such as asymmetry which reduces the efficiency of the transference of shell kinetic energy to fuel potential energy [9]; and S is a scaling parameter applied to all target dimensions as well as time and encompasses the ability of larger capsule surface areas to absorb more energy [10]. Increasing the target scale is straightforward; however, 'hydroscaling' is not universal for all features of the implosion such as gradients, mean free paths, or the laser spot size (i.e., the laser intensity on the hohlraum wall).

Initial experiments at the National Ignition Facility (NIF) [11] showed large quantities of capsule material mixed into the fuel, which prevented the hot spot from reaching high temperature and pressure conditions (figure 1 blue markers) [12, 13]. There is strong evidence for ablation front hydrodynamic instabilities as the source of this mix, in particular those seeded by the large perturbation due to the capsule support engineering feature [14]. Other potential seeds, such as inhomogeneous uptake of oxygen in the ablator, are also under investigation [15]. This issue was mitigated through modifications to the laser pulse increasing the α term but also greatly reducing mix (essentially increasing ϵ). These experiments resulted in the first demonstration of heating via alpha-particle deposition and fusion energy output greater than the energy absorbed by the fuel (figure 1 green markers) [16, 17], a crucial step toward reaching burning plasma and ignition conditions.

Further progress was limited in implosion velocity by laser backscatter out of the hohlraum and hence not available to contribute to the x-ray drive ablating the capsule. Implosions were also limited in efficiency by time-dependent asymmetries induced by cross-beam energy transfer [18, 19], a time-dependent energy transfer process between beams determined by the plasma conditions where the lasers cross at the laser entrance holes on each end of the hohlraum [20]. Near-vacuum or low gas-fill hohlraums address these issues by exhibiting minimal laser backscatter, providing more laser to drive the implosion [21]. Minimal cross-beam energy transfer is also noted when 0 Å beam wavelength separation is used, allowing symmetry to be directly controlled by laser changes as opposed to indirectly controlled through changing plasma conditions. In addition, suprathermal electrons [22], a potential source of increased α, are reduced by two orders of magnitude [21].

To accrue the benefits of low gas-fill hohlraums, experimental campaigns have transitioned to using this category of hohlraum for plastic (CH) shells as well as for beryllium [23–25]. Experiments have also focused on utilizing high density carbon (HDC or polycrystalline diamond) capsules [26–28]. Because HDC is nearly 3× as dense as CH, laser pulses can be 2–3× shorter in length (5–9 ns versus 15–22 ns) and still drive implosions to ignition relevant conditions [29, 30]. HDC experimental campaigns have developed efficient utilization techniques for low gas-fill hohlraums—exploring capsule to hohlraum size [31], time-dependent symmetry control [32, 33], shock timing, and improved stability with capsule dopant [34].

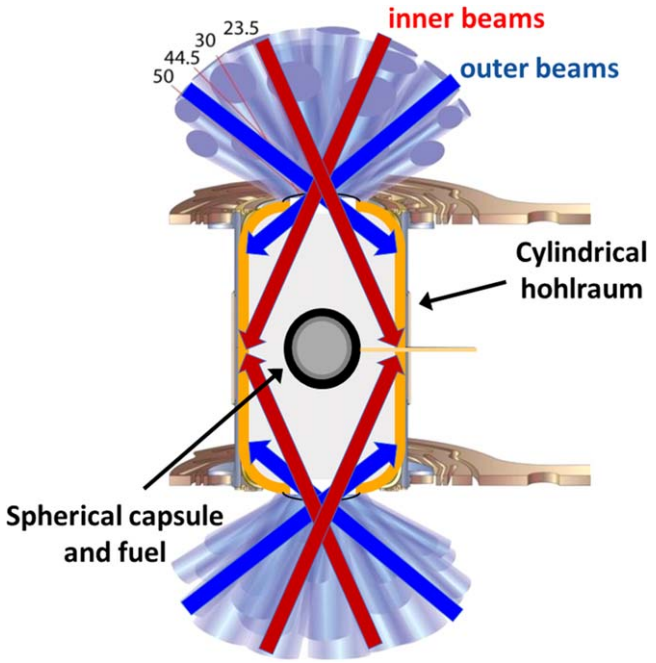

Figure 2. Schematic diagram of target showing capsule and fuel inside hohlraum with inner beams deposition location near the capsule waist and outer beams deposition location near the laser entrance holes; inner and outer beams are in actuality four groups of beams crossing the hohlraum axis at different angles −23° and 30° for inners and 44° and 50° for outers.

In low gas-fill hohlraums, due to the reduced time-dependent cross-beam energy transfer, implosion symmetry is controlled directly through changes in the beam power balance—if more drive is needed on the waist of the capsule, then the 'inner' beams which strike the hohlraum in the equatorial region are increased in power, while if more drive is needed on the poles of the capsule, then the 'outer' beams which strike near the ends of the hohlraum are increased in power (figure 2). Implosion shape is quantified in terms of a Legendre moment decomposition of the 17% contour of peak brightness of measured equatorial x-ray or neutron emission where the zeroth order term (P0) specifies the overall size of the emitting region; P2 specifies the level of oblate or prolateness, and P4 specifies the level of 'square' or 'diamond' shape, as described in [35].

While final implosion shape is important for optimizing nuclear performance, the time-dependent symmetry of the radiation flux producing that shape is of at least equal, if not more, importance [9]. The ultimate goal is to apply minimal P2 (as well as minimal higher orders) throughout the entire drive of the pulse such that the fuel is driven as symmetrically (as efficiently) as possible. As described above, symmetry is controlled through inner and outer beam balance (cone fraction defined as the ratio of inner power to total power). Two-dimensional radiation hydrodynamics simulations with HYDRA including the lasers, hohlraum, and capsule are executed to determine the appropriate cone fraction [36]. The simulated radiation flux striking the capsule can be calculated and decomposed using Legendre polynomials, and the cone fraction modified throughout the laser pulse to maintain

radiation flux P2 near 0 throughout, driving a round ablator and fuel and producing a round hot spot.

The same set of simulations can be used to calculate the P4, set by the geometric locations of the beam spots on the wall. Outer and inner beams can be moved in the simulations to determine the appropriate location which minimizes P4 in the radiation flux and hence in the shell and hot spot. Modes P6 and higher are typically of lesser concern due to the native smoothing which occurs inside a hohlraum [37]. While the goal is to have a completely symmetric implosion, a performance specification has been quantified using 2D HYDRA simulations for the level of implosion P2 and P4 deviation from zero (round) that still produces 70% of the 1D simulated yield at alpha-heating levels of 2× (P2 can deviate ±5 μm, while P4 can deviate ±3 μm) [9].

2. Late-time symmetry control

Typically, hohlraums have been filled with a high density of gas (>1 mg cm^{-3}) to reduce expansion of the hohlraum wall material into the volume of the hohlraum and into the laser beam paths. With a low gas-fill (0.03–0.6 mg cm^{-3}), clear benefits are gained as mentioned [21, 39, 40], but the wall expands readily into the hohlraum volume and into the laser beam paths (figure 3(a)). The challenge of late-time symmetry control is demonstrated in figure 3, where the effects of loss of symmetry control as beams are absorbed in the hohlraum volume are simulated as well as compared to measurements. Radiation flux P2 can be controlled for much of the pulse with cone fraction (figure 3(b), <6 ns), but the inner beams are hindered in their propagation to the hohlraum waist producing a rapid shift to positive P2 (pole hot) in radiation flux near the end of the laser pulse (figure 3(b), 6 ns onwards). The effect on the implosion can be noted in the inset equatorial material density image in figure 3(b); although the outside of the dense shell is relatively round, the internal features show a large build-up of density at the poles resulting in reduced neutron production for this implosion.

Experimentally, one manifestation of this issue can be noted in figure 3(c). The time-resolved measurement of post-bang time x-ray emission provides information regarding the state of the shell convolved with the radiation flux. Although the image at the time of peak neutron emission (bang time) shows a well-formed, albeit oblate implosion, the measured and simulated x-ray emission after bang time indicates significant asymmetry as the outgoing shock interacts with the dense polar features. The agreement between measured and simulated images provides confidence that the radiation flux is understood, both indicating that improvement is needed as well as providing confidence that the simulations can be utilized to determine how that improvement can be achieved.

The challenge of late-time symmetry control has led to laser designs with higher peak power of shorter duration to force the capsule to reach the desired implosion velocity while symmetry control can still be maintained (figure 4). The higher power, shorter pulses allow the capsule to be driven according to design velocity specifications, while being short

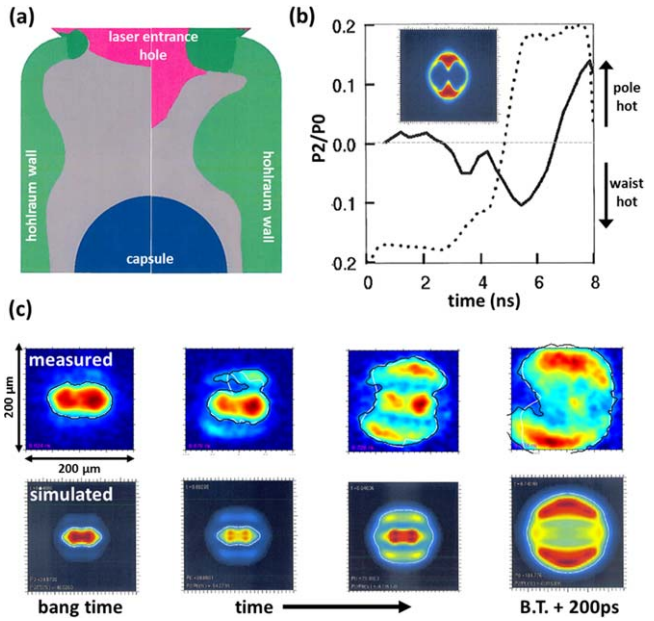

Figure 3. (a) Schematic diagram of upper hohlraum halves showing (left) tamped wall expansion with higher gas-fill or at early time in low-gas fill and (right) late-time expanded wall material; (b) simulated Legendre moment P2 (solid line) of the radiation flux (+P2 flux indicates pole/outer high; −P2 flux indicates waist/inner high) inside the hohlraum applied to the capsule compared to the timing of a laser pulse (dotted line). The inset image is a simulated equatorial material density profile at the time of peak neutron emission showing the result of this radiation flux asymmetry; (c) equatorial x-ray emission images [38] measured from an experiment (N150128, top row) and output from a simulation (bottom row) showing one measurable signature of radiation flux asymmetry, significant density build-up on the poles of the implosion.

enough to avoid the late-time hindrance of inner beam propagation.

With these limitations in mind, a platform has been successfully designed with 5.75 mm diameter, depleted uranium hohlraums filled with 0.3 mg cm^{-3} helium and both W-doped and undoped HDC capsules with 844 μm inner radii, 64 μm thick ablators, and 52 μm thick DT fuel layers ('subscale' targets [32]). Time-dependent P2 symmetry control was achieved and maintained using simulations to guide a changing cone fraction through time. It can be noted, though, as in the lower right image of figure 4 that the hot spot has a degree of 'square' shape indicating a remaining P4 contribution.

Therefore, a series of experiments was executed to demonstrate that P4 could be modified while still keeping P2 within performance specification (figure 5). The spacing of the location of inner versus outer beam spots on the hohlraum wall was steadily widened by moving both the 44° and 50° outer beam groups from a nominal position to +200 μm and to +350 μm toward the laser entrance holes. The shift in P4 was measured by analyzing radiographs of the inflight shell at a convergence of approximately 5× [41]. Through this series, measured P4 clearly shifts and reaches levels within the performance specification showing a sensitivity of ~2 μm of P4 for each 100 μm of outer beam shift. An offset in absolute

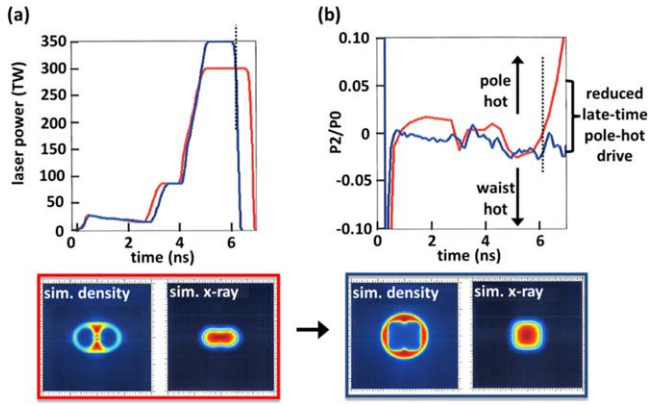

Figure 4. (a) Comparison between two laser pulses which drive similar velocity implosions through different peak power and different lengths; (b) resulting radiation flux from the lower power, longer pulse (red) and the higher power, shorter pulse (blue); images below are simulated equatorial material density and x-ray emission resulting from the longer pulse (red, left) and the shorter pulse (blue, right).

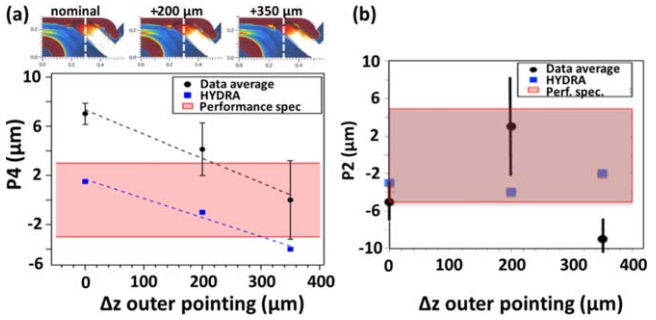

Figure 5. (a) Comparison of measured and simulated P4 values of the inflight shell in a series of experiments (N160119, N160627, N160816) where the outer beams were incrementally moved outward toward the laser entrance holes. Top half-hohlraum diagrams (axes horizontal) display the outer beam location for each experiment; (b) comparison of measured and simulated P2 values corresponding to each experiment.

magnitude of P4 is noted between measurements and simulations, an effect that may indicate inadequate zoning of the simulation wall mesh or possibly non-hydrodynamic, kinetic interactions between the gas fill and hohlraum wall [42]. However, the slope of the shift is consistent between measurements and simulations providing confidence that once an experimental starting point is known the measured P4/outer beam pointing sensitivity can be implemented successfully.

Moving the outer beams toward the laser entrance holes not only affects P4, but will also affect P2 by applying a stronger drive to the poles of the capsule, driving an increasingly oblate radiation flux. Experiments have shown that P2 shifts by 5 μm for each 100 μm shift in outer pointing. Therefore, the balance between the inner and outer beam powers through time must be adjusted as the outer beam spot location is moved. This series of experiments included such cone fraction modifications in addition to the beam pointing changes, and measurements showed that, although P2 did move between experiments, adequate control was maintained.

3. Increased target scale

Building upon these results, the target size was increased by ~8% to 6.2 mm diameter hohlraums, 910 μm HDC capsules' inner radii, 70 μm thick ablators and 56 μm thick DT fuel layers ('midscale' targets) to test the S term in equation (4). The size scaling was indeed effective at increasing yield, reaching new NIF yield to-date records [2], but the symmetry did not scale as nominal 2D radiation hydrodynamics simulations expected. Initial gas-filled capsule experiments ('symcaps' [35]) in midscale targets produced hot spots more oblate than predicted by nominal simulations (figure 6, subscale N160221 was designed and measured to be round while midscale N170206 was designed to be round but measured to be oblate). Further work is needed to fully explain the lack of symmetry scaling, although this effect seems to be caused by a hindrance of late-time laser propagation; one challenge of increasing the scale size of targets is that the laser power and energy must increase to maintain similar hohlraum internal radiation temperature with the increased hohlraum wall area, but the laser spot size cannot increase (beyond a small spread due to the longer path length), thus the laser intensity on the walls increases causing the wall expansion velocity to be higher with larger targets.

To correct the oblate shape, several symmetry control techniques were tested and verified including: increased peak cone fraction, increased hohlraum gas density (0.45 mg cm^{-3} instead of 0.3 mg cm^{-3}), one set of outer beams' (44° beams) pointing shifted inward away from the laser entrance holes (−350 μm), and reduced picket power (44 TW instead of 56 TW). The results of the series of experiments are summarized in figure 6. Due to a limited number of available shots, some experiments changed multiple parameters at once. However, the series taken as a whole can be utilized to interpret distinct sensitivities.

Increased peak power cone fraction forces more drive near the waist of the capsule as the capsule begins to converge without inducing shell to hot spot symmetry swings that reduce ϵ. If simulations underestimate the absorption of the inner beams as the hohlraum is filling with wall and ablator material, then this technique can be effective at empirically correcting for that discrepancy. There is a limit to how much the cone fraction can be increased, though, due to reaching the peak powers deliverable by NIF, and so this technique can only be implemented until that point is reached. Measurements demonstrated that increased peak cone fraction was effective at shifting hot spot symmetry from oblate to round with a sensitivity of ~3 μm per % cone fraction increase.

In simulations, increased hohlraum gas-fill density improves symmetry by slowing the expansion of the hohlraum wall allowing additional late-time inner beam propagation. Experimentally, this effect is not always observed [39], and in fact, the opposite effect where symmetry is more prolate with reduced hohlraum gas-fill density has been distinctly noted [45]. The hohlraum gas-fill density was increased from 0.3 mg cm^{-3} to 0.45 mg cm^{-3}, and the peak

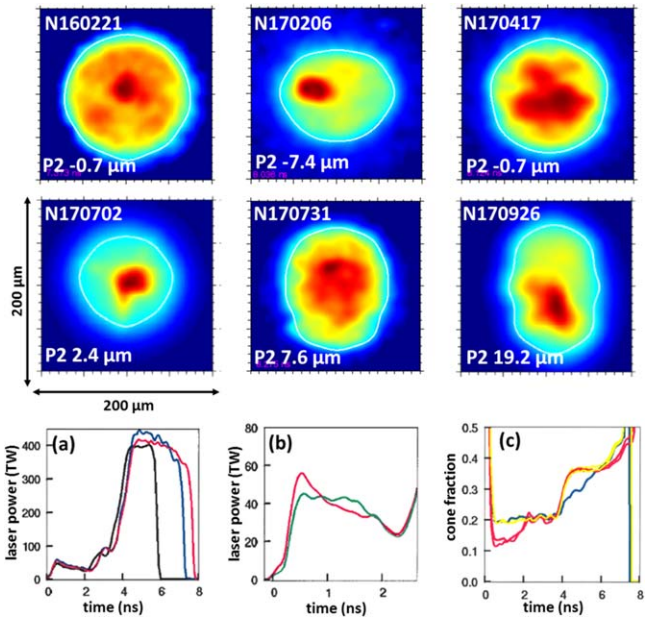

Figure 6. Comparison of measured equatorial x-ray images at bang time through the series of symmetry experiments spanning 'subscale' N160221, 'midscale' 170206, gas density change to 0.45 mg cm^{-3} N170417 with peak cone fraction modification, peak cone fraction modification N170702, pulse length increase with 44° beam pointing modification N170731, and picket reshape N170926. The bright spot noted in the images is attributed to the fuel fill tube [43, 44]; this feature affects the apparent brightness of the underlying hot spot and hence apparent size. However, the P2 in microns remains consistent across multiple brightness contour levels. Laser plots: (a) power versus time comparisons for N160221 (black), N170206, N170417, and N170702 (blue), N170731 and N170926 (red); (b) picket power comparison between N170206, N170702, N170731 (red) and N170926 (green); (c) cone fraction versus time for N170206 (blue), N170417 and N170702 (yellow), and N170731 and N170926 (red).

cone fraction was increased 3%. The resulting hot spot shape did shift toward prolate, but less than the peak cone fraction change alone. This result is consistent with two hypotheses—either the increased gas density cost ~3 μm in P2 or the sensitivity to peak cone fraction is reduced to 2 μm per % cone fraction.

Because longer pulse lengths are more challenging on symmetry, the effect of lengthening peak power (+500 ps) was tested. As this change is expected to push the hot spot shape toward oblate, the separation between the two sets of outer beams was also increased by shifting one set closer to the capsule waist (44° beams only, −350 μm). This separation of the outer beam groups reduces drive on the capsule pole, instead shifting that drive toward the waist and also may reduce the radial extent of the expansion of the wall concentrated near the outer beam deposition location. Previous experiments demonstrated ~5 μm P2 shift per 100 μm of outer beam repoint when both groups of outer beams were shifted. Here, only half of the outer beams were moved, and so the effect can be halved and then scaled to the 350 μm shift yielding an expected P2 total shift of almost 9 μm from the 44° beam repoint. For this experiment, 5 μm of P2 shift was measured. Hence a rough estimate can be made that lengthening the pulse cost ~4 μm of P2. This estimate indicates a sensitivity of ~<1 μm of P2 degradation per 100 ps pulse extension. Simulations with symmetry baselined to the initial oblate implosion were consistent with this level of sensitivity.

To provide further symmetry flexibility, a reduced power picket was implemented. To maximize P2, this picket modification was coupled to 100 μm inward repoint on both the 44° and 50° outer beams. These two changes together induced the largest change in P2 (ΔP2 ~ 12 μm) of the series. As noted, previous experiments have been consistent with ~5 μm P2 shift per 100 μm of outer beam repoint. Therefore, the picket power reduction is consistent with ~7 μm P2 shift for a 20% picket power reduction.

These empirical estimates of picket power effect are consistent with simulation expectations where approximately half of the P2 shift could be seen in simulations with only outer beam repoint and half could be seen in simulations with only picket power reduction. The picket power effect can be interpreted by examining simulations where two contributions are noted. The reduced power picket seems to induce less wall motion, consistent with empirical observations [7]. In addition, the simulations calculate increased cross-beam energy transfer in the peak of the laser pulse caused by altered plasma conditions at the laser entrance holes effectively resulting in a larger peak power cone fraction, already noted to be effective at shifting symmetry.

Although the techniques discussed are focused on late-time symmetry control, early-time control is also key to efficiently driving the implosion. Hence, cone fraction changes were introduced during the foot of the pulse when needed to maintain symmetric shock structure, while still shifting final hot spot shape. The result of this can be seen in figure 6(c) where the picket cone fraction is reduced when the outer beams are repointed. It is also important to note that the level of P4 was not measured to increase outside the performance specification with the separation of the 44° and 50° and with the small repoint.

4. Late-time drive modification

We have designed and experimentally verified several effective symmetry control techniques, but there is another key aspect of experimental performance, a contributor to p_{abl} in equation (4)—the empirical effect of coast time (the time between the end of the laser pulse and peak neutron emission). Previous CH experiments demonstrated a dependence between reduced coast time and increased stagnation pressure. This effect can be noted in figure 1(b) and is consistent with theoretical analysis [46]. Higher power, shorter pulses for late-time symmetry control as discussed here inherently result in a longer delay between the end of the laser pulse and the time of peak neutron emission (longer coast times). While effective at reducing late-time symmetry issues, this laser pulse design has room for improvement to increase expected stagnation pressure.

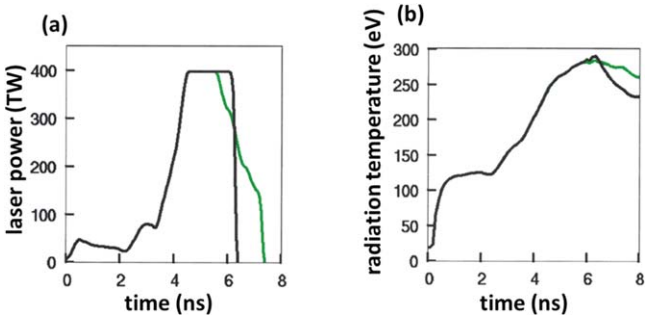

Figure 7. (a) Comparison between a square peak laser pulse (black) and a 'drooping' pulse (green); (b) comparison of the resulting simulated hohlraum internal radiation temperatures between square (black) and 'drooping' pulses (green).

Much research effort has focused on the power and cone fraction history of the laser pulse before peak (in figure 4(a), the pulse before ~5 ns). This additional constraint (reduced coast time) coupled with the inherent late-time symmetry control challenge of low gas-fill hohlraums motivates development of post-peak power laser pulse designs. With the high degree of laser tunability at the NIF, the time history of the laser pulse can indeed be controlled after reaching peak power in addition to the typical control in the earlier time portion.

Reduced coast time through simply lengthening the time at laser peak power returns to the symmetry issue noted in figures 3 and 4 as well as produces an accelerating drive to the capsule rapidly reducing the amount of ablator mass remaining at peak velocity, raising concerns about interface stability and mix.

In fact, three DT layered experiments in the HDC campaign (N141116, N161113, N180218) with varying symmetry, scale, and α have demonstrated that nuclear performance does not increase according to expectations when the mass remaining shrinks to less than ~4%. One design option for modifying the late time laser peak power to reduce coast time but still maintain ablator mass is the 'drooping' drive. Previous point designs [47] explored similar options, but for the first time, we have experimentally explored this design.

Rather than the traditional square laser pulse peak shape, the drooping drive reaches peak power and subsequently ramps down in power extending the pulse later in time. The resulting simulated internal radiation temperature (Tr) changes from a steadily rising, peaked profile to a flattened profile (figure 7(b)). Because the drooping pulse leads to a flattened Tr profile, the capsule does not continue to accelerate and burn mass as with a peaked profile, and the laser pulse is longer, such that short coast times with adequate ablator mass remaining can be designed.

In simulations, the effect of the drooping pulse design is clearly noted (table 1) between two simulations of the same capsule, fuel, and hohlraum with the laser pulses shown in figure 7. Although the drooping pulse is ~1 ns longer, the mass remaining is similar between the two drives. Furthermore, although the fuel velocities are nearly identical, the stagnation pressure is increased 2× with the reduced coast time drive.

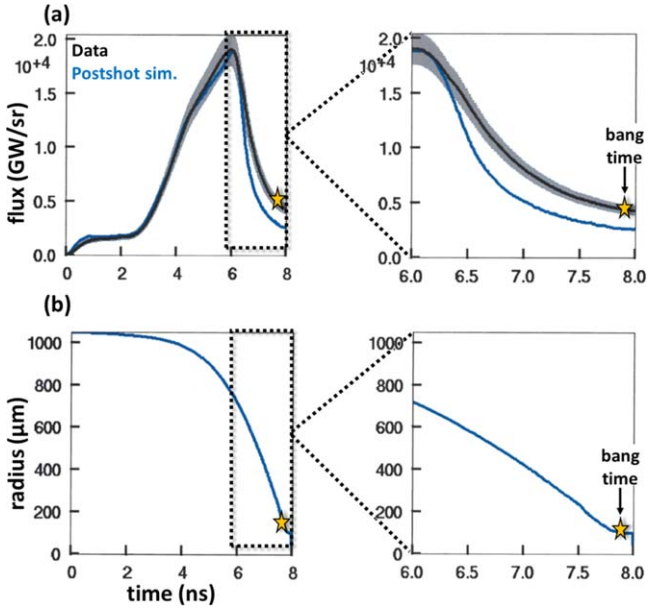

Figure 8. (a) Comparison between a measured Dante flux (black) and a simulation (blue); (b) simulated trajectory of the center of the fuel mass.

Table 1. Comparison of square and 'drooping' pulse implosion metrics.

	Square	Drooping
Bang time (ns)	7.8	7.83
Coast time (ns)	**1.5**	**0.5**
Fuel velocity (km s^{-1})	371	370
DT Tion (keV)	4.7	5.1
Yield	1.3×10^{16}	2.1×10^{16}
Mass remaining	6.8%	6.3%
Stag. pressure (Gbar)	**191**	**343**
ρR (mg cm^{-3})	227	423

The drooping pulse provides an added symmetry benefit in that the late-time peak cone fraction can steadily rise with the decreasing power while still remaining within the NIF laser power delivery capabilities. Effectively, if this cone fraction ramp is utilized, then the inner beams are kept constant through the duration of peak power, while the outer beams are steadily reduced in power. Simulations indicate that this ramping cone fraction improves late-time symmetry control, although this remains to be verified experimentally. Furthermore, laser backscatter often rises late in the pulse and is concentrated in the outer beams; reducing the late-time power in the outer beams can be effective at negating this issue as well.

Moreover, simulations often do not calculate correctly the late time cooling of the hohlraumn noted as a discrepancy between post peak power measured and simulated Dante [48] fluxes (figure 8(a)). With a typical coast time of ~1.8 ns as in figure 8, a significant fraction of the implosion trajectory occurs after the end of the laser pulse when the hohlraum is cooling. Therefore, with the disagreement between measured

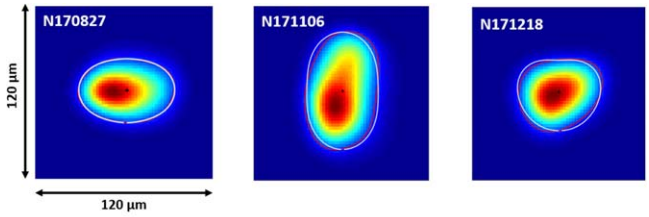

	N170827	N171106	N171218
tot. yield	1.9×10^{16}	1.7×10^{16}	1.7×10^{16}
DSR (%)	3.23	2.95	3.23
P0 μm	28.4	28.7	28.3
P2 μm	-7.6	10.1	-2.5
YOS 2D	30%	47%	33%

Figure 9. Equatorial neutron image [50] comparison for the three DT layered experiments described here (N170827, N171106, N171218) with associated table of measured performance metrics. YOS 2D is a ratio of measured yield to simulated yield from a two-dimensional simulation resolving modes $P < 8$ including the hohlraum, capsule, and delivered laser powers.

and simulated fluxes, this key fraction of the implosion trajectory is subject to hohlraum drive unable to be captured by the simulations. Shrinking the coast time provides higher confidence in simulation fidelity.

5. Robust alpha-heating laser-target combination

Focusing on the laser design aspect of the platform, combining symmetry control techniques with the drooping pulse has led to a controlled and consistent implosion suitable for testing a range of hypotheses for paths to further increase performance. We have executed a series of DT layer experiments to test the effect on performance of symmetry and minor shock timing adjustment. Each implosion reached a similar fuel velocity ($\sim$395 km s^{-1}) and produced similar total neutron yields (figure 9).

Modifying the picket was effective at shifting final hot spot symmetry from oblate to prolate (both in the gas-filled capsules and DT layered experiments), but did not change DT layered implosion performance. Adjusting shock timing (moving the shock mergers away from the capsule:DT ice interface, closer to the ice:gas interface with added picket energy and added trough length) was effective at increasing the down-scatter ratio (DSR, a metric of fuel compression [49]), but again did not change fusion energy output. These results indicate that modest iterations on final symmetry and shock timing are not expected to significantly increase performance, but also that this platform is performing consistently and robustly and is not in a narrow, sensitive region of parameter space.

This robustness is valuable for narrowing the design space over which performance improvements may be expected. The implosion performance is controlled by many factors, including the capsule and hohlraum materials, sizes, and engineering features as well as the power, energy, and time history of the laser pulse. Experiments are underway to further increase S to again test that parameter in equation (4). In addition, there is room for further improvement at the current target scale; despite the robustness of performance, the measured yield over 2D simulated yield remains $<$50%. Sources of that degradation may include perturbation from the fuel fill tube, and so experiments to further shrink the size of that engineering feature are planned. Furthermore, although final measured hot spot symmetry did not affect nuclear performance, simulations indicate that there may be remaining early-time asymmetries due to increased cross-beam transfer with the reduced picket power design; experiments correcting early-time cone fraction could test that simulated effect on performance. Fuel:ablator interface stability coupled with fuel preheat also remains a potentially crucial issue; experiments to optimize capsule dopant for added shielding and improved fuel:ablator stability could be utilized to explore whether this is a contributor to fusion performance. Armed with an increased understanding of symmetry and drive control as detailed here, experimental campaigns will now move forward, building upon these results to attempt to reach the burning plasma regime and beyond.

Acknowledgments

The authors would like to thank the NIF operations, laser, target fabrication, and diagnostic teams for their dedicated efforts during these experiments. This work was performed under the auspices of the US Department of Energy by Lawrence Livermore National Laboratory under Contract DE-AC52-07NA27344 and by General Atomics under Contract DE-NA0001808.

ORCID iDs

L Berzak Hopkins https://orcid.org/0000-0002-9187-5667
O Jones https://orcid.org/0000-0002-0372-7657
M Millot https://orcid.org/0000-0003-4414-3532

References

[1] Lindl J D, Amendt P, Berger R L, Glendinning S G, Glenzer S H, Haan S W, Kauffman R L, Landen O L and Suter L J 2004 The physics basis for ignition using indirect-drive targets on the national ignition facility *Phys. Plasmas* **11** 339–491

[2] Le Pape S *et al* 2018 Fusion energy output greater than the kinetic energy of an imploding shell at the national ignition facility *Phys. Rev. Lett.* **120** 245003

[3] Kemp A, Meyer-ter Vehn J and Atzeni S 2001 Stagnation pressure of imploding shells and ignition energy scaling of inertial confinement fusion targets *Phys. Rev. Lett.* **86** 3336–9

[4] Spears B K *et al* 2012 Performance metrics for inertial confinement fusion implosions: aspects of the technical framework for measuring progress in the national ignition campaign *Phys. Plasmas* **19** 056316

[5] Betti R, Christopherson A R, Spears B K, Nora R, Bose A, Howard J, Woo K M, Edwards M J and Sanz J 2015 Alpha heating and burning plasmas in inertial confinement fusion *Phys. Rev. Lett.* **114** 255003

[6] Christensen-Dalsgaard J and Berthomieu G 1991 *Solar Interior and Atmosphere* (Tucson: University of Arizona Press)

[7] Callahan D A *et al* 2018 Exploring the limits of case-to-capsule ratio, pulse length, and picket energy for symmetric hohlraum drive on the national ignition facility laser *Phys. Plasmas* **25** 056305

[8] Haan S W *et al* 2011 Point design targets, specifications, and requirements for the 2010 ignition campaign on the national ignition facility *Phys. Plasmas* **18** 051001

[9] Kritcher A L *et al* 2014 Metrics for long wavelength asymmetries in inertial confinement fusion implosions on the national ignition facility *Phys. Plasmas* **21** 042708

[10] Nora R *et al* 2014 Theory of hydro-equivalent ignition for inertial fusion and its applications to omega and the national ignition facility *Phys. Plasmas* **21** 056316

[11] Miller G H, Moses E I and Wuest C R 2004 The national ignition facility: enabling fusion ignition for the 21st century *Nucl. Fusion* **44** S228

[12] Edwards M J *et al* 2013 Progress towards ignition on the national ignition facility *Phys. Plasmas* **20** 070501

[13] Ma T *et al* 2013 Onset of hydrodynamic mix in high-velocity, highly compressed inertial confinement fusion implosions *Phys. Rev. Lett.* **111** 085004

[14] Clark D S *et al* 2016 Three-dimensional simulations of low foot and high foot implosion experiments on the national ignition facility *Phys. Plasmas* **23** 056302

[15] Haan S W, Huang H, Johnson M A, Stadermann M, Baxamusa S, Bhandarkar S, Clark D S, Smalyuk V and Robey H F 2015 Instability growth seeded by oxygen in ch shells on the national ignition facility *Phys. Plasmas* **22** 032708

[16] Hurricane O A *et al* 2014 Fuel gain exceeding unity in an inertially confined fusion implosion *Nature* **506** 343–8

[17] Meezan N B *et al* 2017 Indirect drive ignition at the national ignition facility *Plasma Phys. Control. Fusion* **59** 014021

[18] Pak A *et al* 2017 Examining the radiation drive asymmetries present in the high foot series of implosion experiments at the national ignition facility *Phys. Plasmas* **24** 056306

[19] Kritcher A L *et al* 2016 Integrated modeling of cryogenic layered highfoot experiments at the nif *Phys. Plasmas* **23** 052709

[20] Michel P *et al* 2009 Tuning the implosion symmetry of icf targets via controlled crossed-beam energy transfer *Phys. Rev. Lett.* **102** 025004

[21] Berzak Hopkins L F *et al* 2015 First high-convergence cryogenic implosion in a near-vacuum hohlraum *Phys. Rev. Lett.* **114** 175001

[22] Robey H F *et al* 2014 Shock timing measurements and analysis in deuterium–tritium-ice layered capsule implosions on nif *Phys. Plasmas* **21** 022703

[23] Hinkel D E *et al* 2016 Development of improved radiation drive environment for high foot implosions at the national ignition facility *Phys. Rev. Lett.* **117** 225002

[24] Simakov A N *et al* 2017 Performance of beryllium targets with full-scale capsules in low-fill 6.72 mm hohlraums on the national ignition facility *Phys. Plasmas* **24** 052704

[25] Kritcher A L *et al* 2018 Comparison of plastic, high density carbon, and beryllium as indirect drive nif ablators *Phys. Plasmas* **25** 056309

[26] Biener J *et al* 2009 Diamond spheres for inertial confinement fusion *Nucl. Fusion* **49** 112001

[27] Biener M M *et al* 2010 Controlled incorporation of mid-to-high z transition metals in cvd diamond *Diam. Relat. Mater.* **19** 643–7

[28] Casey D T *et al* 2018 The high velocity, high adiabat, bigfoot campaign and tests of indirect-drive implosion scaling *Phys. Plasmas* **25** 056308

[29] Ho D D, Haan S W, Salmonson J D, Clark D S, Lindl J D, Milovich J L, Thomas C A, Berzak Hopkins L F and Meezan N B 2016 Implosion configurations for robust ignition using high- density carbon (diamond) ablator for indirect-drive icf at the national ignition facility *J. Phys.: Conf. Ser.* **717** 012023

[30] MacKinnon A J *et al* 2014 High-density carbon ablator experiments on the national ignition facilitya) *Phys. Plasmas* **21** 056318

[31] Le Pape S *et al* 2016 The near vacuum hohlraum campaign at the nif: a new approach *Phys. Plasmas* **23** 056311

[32] Divol L *et al* 2017 Symmetry control of an indirectly driven high-density-carbon implosion at high convergence and high velocity *Phys. Plasmas* **24** 056309

[33] Turnbull D *et al* 2016 Symmetry control in subscale near-vacuum hohlraums *Phys. Plasmas* **23** 052710

[34] Berzak Hopkins L *et al* 2018 Increasing stagnation pressure and thermonuclear performance of inertial confinement fusion capsules by the introduction of a high-z dopant *Plasma Lett.* accepted

[35] Kyrala G A *et al* 2011 Symmetry tuning for ignition capsules via the symcap technique *Phys. Plasmas* **18** 056307

[36] Marinak M M, Kerbel G D, Gentile N A, Jones O, Munro D, Pollaine S, Dittrich T R and Haan S W 2001 Three-dimensional hydra simulations of national ignition facility targets *Phys. Plasmas* **8** 2275–80

[37] Lindl J D 1998 *Inertial Confinement Fusion* (Berlin: Springer)

[38] Oertel J A *et al* 2006 Gated x-ray detector for the national ignition facility *Rev. Sci. Instrum.* **77** 10E308

[39] Hall G N *et al* 2017 The relationship between gas fill density and hohlraum drive performance at the national ignition facility *Phys. Plasmas* **24** 052706

[40] Jones O S *et al* 2016 Towards a more universal understanding of radiation drive in gas-filled hohlraums *J. Phys.: Conf. Ser.* **717** 012026

[41] Rygg J R *et al* 2014 2d x-ray radiography of imploding capsules at the national ignition facility *Phys. Rev. Lett.* **112** 195001

[42] Rinderknecht H G, Amendt P A, Wilks S C and Collins G 2018 Kinetic physics in icf: present understanding and future directions *Plasma Phys. Control. Fusion* **60** 064001

[43] MacPhee A G *et al* 2017 X-ray shadow imprint of hydrodynamic instabilities on the surface of inertial confinement fusion capsules by the fuel fill tube *Phys. Rev. E* **95** 031204

[44] Pak A *et al* 2018 Impact of fill tube perturbation on implosion experiments conducted with high density carbon ablators, private communication
[45] Berzak Hopkins L *et al* 2015 Near-vacuum hohlraums for driving fusion implosions with high density carbon ablators *Phys. Plasmas* **22** 056318
[46] Hurricane O A *et al* 2017 On the importance of minimizing coast-time in x-ray driven inertially confined fusion implosions *Phys. Plasmas* **24** 092706
[47] Haan S W *et al* 1995 Design and modeling of ignition targets for the national ignition facility *Phys. Plasmas* **2** 2480–7
[48] Dewald E L *et al* 2004 Dante soft x-ray power diagnostic for national ignition facility *Rev. Sci. Instrum.* **75** 3759–61
[49] Gatu Johnson M *et al* 2012 Neutron spectrometryan essential tool for diagnosing implosions at the national ignition facility (invited) *Rev. Sci. Instrum.* **83** 10D308
[50] Merrill F E *et al* 2012 The neutron imaging diagnostic at NIF (invited) *Rev. Sci. Instrum.* **83** 10D317